

Fractional quantum anomalous Hall and anyon density-wave halo in a minimal interacting lattice model of twisted bilayer MoTe₂

Chuyi Tuo,¹ Ming-Rui Li,¹ and Hong Yao^{1,*}

¹*Institute for Advanced Study, Tsinghua University, Beijing 100084, China*

(Dated: December 30, 2025)

The experimental discovery of fractional quantum anomalous Hall (FQAH) states in tunable moiré superlattices has sparked intense interest in exploring the interplay between topological order and symmetry breaking phases. In this paper, we present a comprehensive numerical study of this interplay through large-scale density matrix renormalization group (DMRG) simulations on a minimal two-band lattice model of twisted bilayer MoTe₂ at filling $\nu = -2/3$. We find robust FQAH ground states and provide clear numerical evidences for anyon excitations with fractional charge and pronounced real-space density modulations, directly supporting the recently proposed anyon density-wave halo picture. We also map out the displacement field dependent phase diagram, uncovering a rich landscape of charge ordered states emerging from the FQAH, including a quantum anomalous Hall crystal (QAHC) with an integer quantized Hall conductance. We expect our work to inspire further research interest of intertwined correlated topological phases in moiré systems.

Introduction.—The fractional quantum Hall effect (FQHE) [1–5] represents one of the most profound phenomena in modern condensed matter physics, offering a canonical example of intrinsic topological order [6] characterized by fractionalized anyon excitations [2, 7], topological ground state degeneracy [8], emergent gauge field [9], and long-range quantum entanglement [10, 11]. While traditional studies of the FQHE have largely focused on two-dimensional electron gases under strong magnetic fields, its zero field analog on lattice systems, the FQAH state, has long been theoretically anticipated to emerge in bands with nontrivial Chern numbers [12–19] and favorable quantum geometry [20–25]. Very recently, breakthrough in moiré van der Waals heterostructures [26–34] have enabled the experimental realization of FQAH in various experimental systems. Following initial signatures in twisted bilayer graphene under a small magnetic field [35], robust zero-field FQAH have been decisively observed in twisted bilayer MoTe₂ (*t*MoTe₂) [36–42] and in aligned multilayer rhombohedral graphene/hBN [43–55], sparking a surge of interest in the microscopic mechanisms governing these correlated topological phases [56–117].

FQAH in *t*MoTe₂ feature a much richer interplay between topological order and symmetry breaking than their FQHE counterparts [107]. Unlike Landau levels where kinetic energy is quenched, FQAH emerges from moiré Chern bands that generally possess finite dispersion. This introduces a kinetic energy scale that competes with interactions, promoting a delicate intertwining between FQAH and proximate ordered states, such as charge density waves (CDWs) [36–42] or even unconventional superconductivity [42]. One particularly compelling theoretical proposal capturing this intertwining suggests that anyons can nucleate a halo of proximate CDW order [108], rendering them extended objects with nontrivial internal structure and offering a new perspective on how FQAH give way to other competing phases.

On the other hand, in moiré superlattice systems, transitions between FQAH and charge ordered phases are often driven by the displacement field, making it crucial for understanding the relationship between topological order and charge orders. One particularly intriguing scenario is the emergence of a QAHC [76, 107, 109–117], where the onset of charge order reshapes the topological response, converting a fractional Hall conductance into an integer one. Despite the fundamental importance of both anyon internal structures and displacement field effects, investigating these phenomena has been hindered by limited system size of exact diagonalization [56–75], and large-scale many-body simulations remain scarce [62, 76–79].

In this paper, we directly address the intertwined FQAH-CDW physics by employing large-scale DMRG [118–120] simulations on a minimal interacting lattice model, focusing on the paradigmatic moiré FQAH system of 3.7° *t*MoTe₂ at filling $\nu = -2/3$. The real-space hopping parameters are obtained through Wannierization [60, 121–123] to accurately reproduce the continuum model band structure, while nearest-neighbor (NN) and next-nearest-neighbor (NNN) interactions, together with the displacement field, are treated as tunable parameters. We first demonstrate that robust FQAH ground state can already be stabilized in a minimal model with NN interactions only. By introducing single particle doping into the FQAH ground state, we obtain clear numerical evidence for fractionalized anyon excitations with density-wave halo [108] internal structure. By further including NNN interactions and the displacement field, we map out the resulting phase diagram, revealing that both QAHC and topologically trivial CDW phases can be stabilized. Our findings establish a concrete microscopic framework for understanding the intertwined topological and symmetry breaking physics in moiré superlattice systems.

Model and methods.—Our starting point is the continuum model [28] for 3.7° *t*MoTe₂, which is typically formulated in momentum space and has been widely used

to study the moiré band structure and many-body properties. However, this formulation is not directly compatible with many-body methods like DMRG, which generally require a real space tight-binding representation. To bridge this gap, we construct Wannier orbitals via Wannierization [124], and we restrict to spinless fermion model due to the robust experimental evidence of spin-valley polarized ferromagnetism [125]. Since the top-most moiré valence band carries a non-zero Chern number ($C = -1$), we incorporate the second valence band ($C = +1$) to eliminate the topological Wannier obstruction. Leveraging the layer-polarization inherent to stacking of transition metal dichalcogenides, we can obtain two exponentially localized Wannier functions in a more convenient way [60, 121–124]. The resulting two orbitals are shown in Fig. 1(a), where they are localized around the Wannier centers ($\pm a_M/2\sqrt{3}, 0$), forming a honeycomb lattice, with A orbital predominantly on the top layer and B orbital on the bottom layer, as expected.

With the Wannier functions, we construct a real space tight-binding model:

$$H_0 = \sum_{ij} t_{ij} c_i^\dagger c_j \quad (1)$$

where t_{ij} denotes the hopping amplitude between sites i and j , and c_i^\dagger is the creation operator for a spinless fermion at K valley. By retaining up to the fifth-nearest-neighbor hopping with parameters $(t_1, t_2, t_3, t_4, t_5) = (-3.88, 1.93e^{i2\pi/3}, 0.94, -0.34, -0.13)$ meV (see hopping patterns in Fig. 1(c)), we obtain a tight-binding model that takes the form of a generalized Haldane model [126] and faithfully reproduces the dispersion of the continuum model, as shown in Fig. 1(b).

Next, we address the interaction effects and the influence of the displacement field. In contrast to the single-particle band structure, determining the precise form and strength of interactions is challenging due to the complex screening environment in moiré systems. Therefore, we focus on a minimal model where only the NN and NNN interactions are retained:

$$H_{\text{int}} = V_1 \sum_{\langle ij \rangle} n_i n_j + V_2 \sum_{\langle\langle ij \rangle\rangle} n_i n_j \quad (2)$$

where V_1, V_2 are the strength of NN and NNN interaction, and n_i represent the density at site i . This approximation is justified when the screening effects in $t\text{MoTe}_2$ are strong enough to suppress longer-range components. Moreover, due to the layer polarization of the Wannier functions, the displacement field effects can be captured as a sublattice staggered potential:

$$H_D = D \sum_i (-1)^i n_i, \quad (3)$$

where $(-1)^i = \pm 1$ for $i \in A/B$ sublattice, D denotes the strength of the displacement field. The full interacting Hamiltonian is thus given as $H = H_0 + H_{\text{int}} + H_D$.

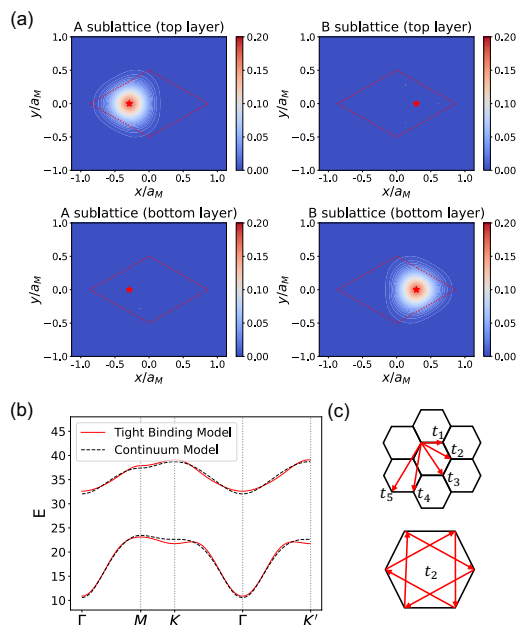


FIG. 1. (a) Density distribution of the Wannier functions, with Wannier centers indicated by stars and moiré unit cell shown as dashed line. (b) Comparison of the band structure between the tight-binding model and the continuum model. (c) Illustration of the hopping terms in tight-binding model on a honeycomb lattice. The next nearest neighbor hopping t_2 carry phase $+2\pi/3$ along the indicated arrow direction.

To investigate the interacting physics of the model, we employ the DMRG algorithm, which is well suited for studying the interplay between topology and strong correlations. In our simulations, we exploit $U(1)$ charge conservation symmetry, with the total particle number is chosen to ensure the correct bulk filling $\nu = -2/3$. We adopt $L_y = 6$ cylinder geometry, and keep bond dimensions up to $\chi = 4000$, which is sufficient to accurately extract the ground state properties of the system.

FQAH state.—We begin by examining whether a minimal model of $t\text{MoTe}_2$ can realize a FQAH phase at $\nu = -2/3$, focusing on small to intermediate NN repulsion V_1 regime, while keeping both NNN repulsion V_2 and the displacement field D at zero. Fig. 2(a) illustrates the single particle Green's functions $\langle c_i^\dagger c_j \rangle$, which reveal a sharp qualitative distinction between the weak and intermediate interaction regimes. For $V_1 < 8$ meV, the Green's functions decay algebraically, a characteristic of Fermi liquid behavior. In contrast, for $V_1 \geq 8$ meV, it exhibits a rapid exponential decay, indicating the onset of an insulating state with a finite single particle gap.

To elucidate the nature of this insulator, we examine the real-space density profile for a representative case at $V_1 = 8$ meV, as shown in Fig. 2(b) and (c). Except for the boundary, the bulk density is pinned exactly at $\langle n \rangle = 2/3$, consistent with the featureless, translationally invariant nature expected for a FQAH state. Fig. 2(d)

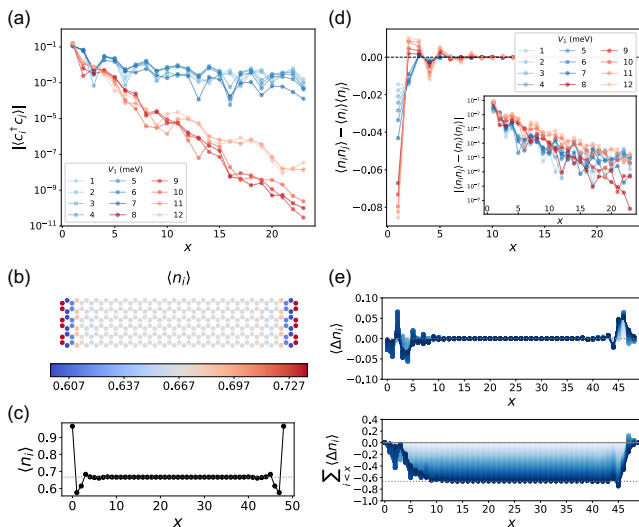


FIG. 2. (a) Single particle Green's functions for various NN interaction V_1 . (b) Real space density profile $\langle n_i \rangle$ at $V_1 = 8$ meV. (c) The same density distribution averaged along y direction. (d) Connected density correlations for different NN interaction V_1 in linear (semi-log) scale for main (inset) figure. (e) Adiabatic charge pumping under insertion of 2π flux thread through the cylinder at $V_1 = 8$ meV. The upper panel shows the local density change, while the lower panel shows its cumulative sum from the left boundary, where the color shading indicates the magnitudes of the inserted flux.

further demonstrates the connected density correlations $\langle n_i n_j \rangle - \langle n_i \rangle \langle n_j \rangle$ for different interaction V_1 . The inset reveals that the decay behavior changes qualitatively from algebraic ($V_1 < 8$ meV) to exponential ($V_1 \geq 8$ meV), consistent with a transition into fully gapped state. Moreover, the main panel highlights that the NN density correlations are strongly suppressed in the insulating regime, reflecting local electron avoidance and the formation of a correlation hole, consistent with FQAH physics.

While the density profile and correlations strongly suggest a FQAH phase, a definitive confirmation requires direct probing the topological properties. The DMRG simulations on cylinder geometry offer a natural framework for accessing Hall conductance of the system through Laughlin's adiabatic charge pumping via flux insertion [124, 127–130]. The presence of nearby competing states makes a sufficiently slow flux insertion essential. Accordingly, we employ a system with length $L_x = 49$ and discretize the 2π flux insertion into 100 steps, while retaining the bond dimension to $\chi = 1000$ to maintain computational feasibility. As shown in Fig. 2(e), for the $V_1 = 8$ meV system, adiabatically threading a 2π flux through the cylinder induces density changes localized at the edges, while leaving the bulk density invariant. This process results in a net charge transfer of exactly $\Delta Q = 2/3$ from the left edge to the right edge, corresponding to a fractionally quantized Hall conductance

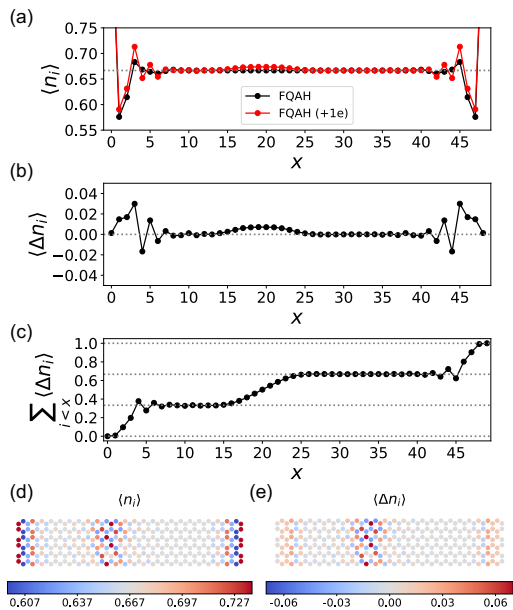


FIG. 3. (a) y -direction averaged real space density profile for the FQAH at $V_1 = 8$ meV (black) and for the system with one added electron (red). (b) Density difference $\langle \Delta n_i \rangle$ between these two systems. (c) Cumulative sum of the density difference from the left boundary. The gray dashed lines at 0, 1/3, 2/3, 1 mark the expected fractionally quantized value of charge. (d) Real space density distribution for the added-electron system in (a). (e) Real space distribution for the density difference in (b).

of $\sigma_{xy} = -2/3$. Taken together, these numerical observations provide unambiguous evidence that our $t\text{MoTe}_2$ model, even with only NN repulsion V_1 , hosts a robust FQAH ground state.

Anyon density-wave halo.—Beyond the fractionally quantized Hall conductance, another definitive hallmark of intrinsic topological order of FQAH phase is the existence of fractionalized anyon excitations. Our DMRG simulations directly demonstrate this fractionalization by introducing a single electron into the FQAH ground state. Fig. 3(a) presents the density distribution for the FQAH state at $V_1 = 8$ meV and for the system with one extra electron, and Fig. 3(b) shows the resulting density difference. These results clearly reveal that the added single electron charge separates into three spatially distinct regions, two located at the boundaries and one inside the bulk, which is indicative of three anyon excitations. To unambiguously verify the fractional nature of these excitations, we calculate the cumulative sum of the density difference starting from the left boundary, as shown in Fig. 3(c). This profile clearly demonstrates that each region carries precisely 1/3 of the electron charge, consistent with the expected fractionalization of FQAH at $\nu = -2/3$. These findings confirm that doping the FQAH system injects fractionalized anyons rather than electrons into the system.

The ability to spatially isolate a single anyon provides a unique opportunity to numerically resolve its internal structure. Fig. 3(d) and (e) show the real space density for the doped system and the corresponding density difference associated with the anyon charge distribution. Crucially, the anyons exhibit strong real-space density modulations, consistent with the recently proposed anyon density-wave halo picture [108]. In this framework, the internal modulation reflects the proximity to a charge ordered phase. Specifically, if the FQAH state is viewed as a condensate of composite bosons, the anyon corresponds to a vortex defect. Within the vortex core, the condensate amplitude is suppressed, allowing the competing density-wave order to manifest. We further demonstrate that such anyon density-wave halo persists for finite NNN interaction V_2 and displacement field D with a much cleaner charge order pattern [124]. This phenomenon highlights the intricate interplay between the FQAH phase and the proximate charge ordered phases.

Displacement field effects.—We now turn to the role of the displacement field in $t\text{MoTe}_2$, which drives transitions between the FQAH and competing charge ordered phases. By keeping NN repulsion at a representative value of $V_1 = 10$ meV and additionally incorporating the NNN repulsion V_2 , we uncover a rich landscape of ground states, as summarized in Fig. 4(a), hosting the FQAH phase, two $\sqrt{3} \times \sqrt{3}$ CDW phases with distinct topological character (i.e. QAHC and CDW), a stripe phase, and a layer polarized (LP) phase. Within this phase diagram, the FQAH phase identified previously remains stable against finite NNN interaction V_2 and displacement field D , as expected from the robustness of the fully gapped topological order. While a finite displacement field induces weak sublattice staggered density modulations, it does not immediately destroy the topological order. Notably, the inclusion of weak NNN repulsion V_2 serves to further stabilize the FQAH phase.

In the regime of weak V_2 , increasing the displacement field D drives a transition from the FQAH phase into a stripe phase. A representative real space density distribution for the stripe phase is shown in Fig. 4(b), which exhibits unidirectional charge modulation with a period of approximately three unit cells along the x -direction. With further increase of D , the stripe pattern melts, and the system eventually transitions into a LP phase, where the electrons are almost entirely confined to a single sublattice in response to the strong displacement field. To shed light on the transport properties of these phases, Fig. 4(e) shows the single particle Green's function at $V_2 = 0$ meV for various displacement fields, revealing insulating behavior in the stripe phase and metallic behavior in the LP phase. This metallic behavior can be understood from an effective model on the hole-rich sublattice in the large displacement field limit, where the NNN interaction V_2 is insufficient to destabilize the Fermi liquid behavior.

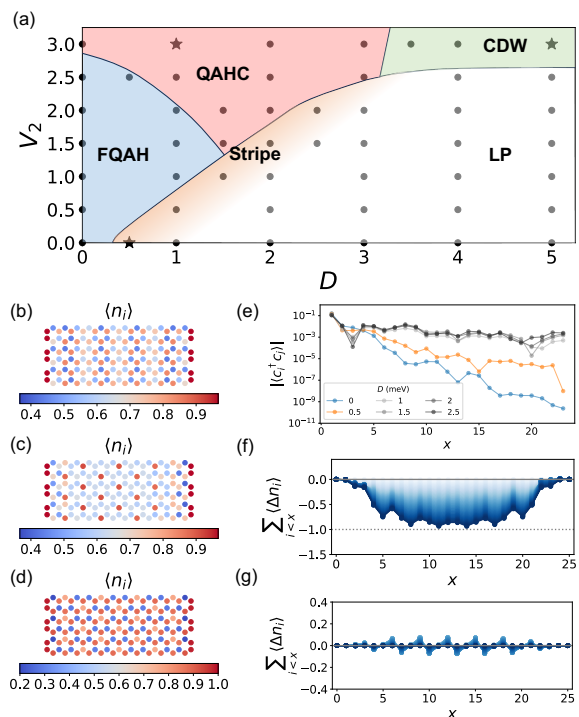


FIG. 4. (a) Ground state phase diagram as a function of NNN interaction V_2 and displacement field D at fixed NN interaction $V_1 = 10$ meV, obtained using $L_x = 25$ cylinders. The stripe region is depicted only schematically by an orange shade. (b-d) Real space density distribution $\langle n_i \rangle$ for three representative systems in different charge ordered phases marked by stars in the phase diagram: (b) $V_2 = 0$ meV, $D = 0.5$ meV; (c) $V_2 = 3$ meV, $D = 1$ meV; (d) $V_2 = 3$ meV, $D = 5$ meV. (e) Single particle Green's functions $\langle c_i^\dagger c_j \rangle$ for various displacement fields D at $V_1 = 10$ meV and $V_2 = 0$ meV, obtained from $L_x = 49$ cylinders. (f, g) Adiabatic charge pumping under insertion of 2π flux for the same representative systems as in (c) and (d), where the color shading indicates the magnitudes of the inserted flux.

For sufficiently large V_2 , the system favors the formation of $\sqrt{3} \times \sqrt{3}$ CDW phases. In our simulations, we identify two qualitatively distinct CDW patterns, with representative real-space density distributions presented in Fig. 4(c) and (d), and the transition between them appears to be first order. Although these two CDW phases are not distinguished by symmetry, they differ in whether the spontaneous translational symmetry breaking predominantly occurs on the hole-poor or hole-rich sublattice. Moreover, adiabatic charge pumping simulations indicate that the two CDW phases differ qualitatively in their topological properties. Fig. 4(f) shows the charge pumping at the representative system with $V_2 = 3$ meV and $D = 1$ meV, where adiabatically threading a 2π flux through the cylinder induces an integer net charge transfer $\Delta Q = 1$ from the left edge to the right edge, demonstrating that the system realizes a QAHC phase in this parameter regime with both CDW order and integer

quantized Hall conductance $\sigma_{xy} = -1$. However, performing the same adiabatic charge pumping procedure at $V_2 = 3$ meV and $D = 5$ meV shows no evidence of net charge transfer, suggesting a topologically trivial CDW phase. Taken together, the displacement field serves as an indispensable tuning parameter that gives rise to a rich set of ground states in $t\text{MoTe}_2$.

Summary and outlook.—In this paper, we present a comprehensive microscopic study of the interplay between FQAH and charge orders in $t\text{MoTe}_2$. By performing large-scale DMRG simulations on a minimal interacting lattice model, we provide clear numerical evidences for robust FQAH ground state, anyon density-wave halo, and a rich displacement-field tunable ground state landscape. These results provide valuable insight from both theoretical and experimental perspectives.

One central implication of our results is that, FQAH and charge order in $t\text{MoTe}_2$ do not merely compete energetically, but intertwine non-trivially via the internal structure of excitations. This observation aligns remarkably well with the anyon density-wave halo picture proposed recently by Song and Senthil [108]. Such intertwining nontrivially reshapes the low-energy effective theory and has far-reaching implications. One prominent consequence is that, defects in the nearby CDW phase can carry fractional charge and orbital magnetization, reflecting the proximity to the underlying FQAH phase, which deserves future numerical and experimental verification.

Experimentally, our ground state phase diagram on displacement field effects (Fig. 4(a)) has direct relevance for interpreting the recent observations in $t\text{MoTe}_2$. Near the $\nu = -2/3$ FQAH state, recent experiments have reported a pronounced anomalous Hall response and several reentrant integer quantum anomalous Hall states as the filling factor and displacement field are tuned [42]. This phenomenology is naturally related to the broad QAHC region in our phase diagram. An important open question is whether such QAHC with integer quantized Hall conductance can be stabilized exactly at the fractional filling $\nu = -2/3$ in future experiments of $t\text{MoTe}_2$. At larger displacement fields, our phase diagram suggests a topologically trivial CDW state, consistent with the insulating behavior observed experimentally. Looking forward, another intriguing open question is whether the unconventional superconductivity recently observed in $t\text{MoTe}_2$ [42] can be understood within this or related microscopic frameworks [131–141]. We believe our work will stimulate further theoretical and experimental interest in investigating the intertwined nature of correlated topological phases in moiré systems.

Acknowledgments.—We thank Xue-Yang Song for helpful discussions. This work is supported in part by MOSTC under Grant No. 2021YFA1400100 (H.Y.), by NSFC under Grant Nos. 12347107 (C.T., M.-R.L., H.Y.) and 12334003 (H.Y.), and by the New Cornerstone Science Foundation through the Xplorer Prize (H.Y.).

* yaohong@tsinghua.edu.cn

- [1] D. C. Tsui, H. L. Stormer, and A. C. Gossard, Two-dimensional magnetotransport in the extreme quantum limit, *Phys. Rev. Lett.* **48**, 1559 (1982).
- [2] R. B. Laughlin, Anomalous quantum hall effect: An incompressible quantum fluid with fractionally charged excitations, *Phys. Rev. Lett.* **50**, 1395 (1983).
- [3] F. D. M. Haldane, Fractional quantization of the hall effect: A hierarchy of incompressible quantum fluid states, *Phys. Rev. Lett.* **51**, 605 (1983).
- [4] J. K. Jain, Composite-fermion approach for the fractional quantum hall effect, *Phys. Rev. Lett.* **63**, 199 (1989).
- [5] S. Kivelson, D.-H. Lee, and S.-C. Zhang, Global phase diagram in the quantum hall effect, *Phys. Rev. B* **46**, 2223 (1992).
- [6] X.-G. Wen, Topological orders in rigid states, *Int. J. Mod. Phys. B* **4**, 239 (1990).
- [7] D. Arovas, J. R. Schrieffer, and F. Wilczek, Fractional statistics and the quantum hall effect, *Phys. Rev. Lett.* **53**, 722 (1984).
- [8] X.-G. Wen and Q. Niu, Ground-state degeneracy of the fractional quantum hall states in the presence of a random potential and on high-genus riemann surfaces, *Phys. Rev. B* **41**, 9377 (1990).
- [9] S. C. Zhang, T. H. Hansson, and S. Kivelson, Effective-field-theory model for the fractional quantum hall effect, *Phys. Rev. Lett.* **62**, 82 (1989).
- [10] A. Kitaev and J. Preskill, Topological entanglement entropy, *Phys. Rev. Lett.* **96**, 110404 (2006).
- [11] M. Levin and X.-G. Wen, Detecting topological order in a ground state wave function, *Phys. Rev. Lett.* **96**, 110405 (2006).
- [12] E. Tang, J.-W. Mei, and X.-G. Wen, High-temperature fractional quantum hall states, *Phys. Rev. Lett.* **106**, 236802 (2011).
- [13] K. Sun, Z. Gu, H. Katsura, and S. Das Sarma, Nearly flatbands with nontrivial topology, *Phys. Rev. Lett.* **106**, 236803 (2011).
- [14] T. Neupert, L. Santos, C. Chamon, and C. Mudry, Fractional quantum hall states at zero magnetic field, *Phys. Rev. Lett.* **106**, 236804 (2011).
- [15] D. N. Sheng, Z.-C. Gu, K. Sun, and L. Sheng, Fractional quantum hall effect in the absence of landau levels, *Nature Communications* **2**, 389 (2011).
- [16] N. Regnault and B. A. Bernevig, Fractional chern insulator, *Phys. Rev. X* **1**, 021014 (2011).
- [17] E. J. Bergholtz and Z. Liu, Topological flat band models and fractional chern insulators, *Int. J. Mod. Phys. B* **27**, 1330017 (2013).
- [18] Y.-F. Wang, H. Yao, Z.-C. Gu, C.-D. Gong, and D. N. Sheng, Non-abelian quantum hall effect in topological flat bands, *Phys. Rev. Lett.* **108**, 126805 (2012).
- [19] Y.-F. Wang, H. Yao, C.-D. Gong, and D. N. Sheng, Fractional quantum hall effect in topological flat bands with chern number two, *Phys. Rev. B* **86**, 201101 (2012).
- [20] R. Roy, Band geometry of fractional topological insulators, *Phys. Rev. B* **90**, 165139 (2014).
- [21] P. J. Ledwith, G. Tarnopolsky, E. Khalaf, and A. Vishwanath, Fractional chern insulator states in twisted bilayer graphene: An analytical approach, *Phys. Rev. Re-*

- search **2**, 023237 (2020).
- [22] J. Wang, J. Cano, A. J. Millis, Z. Liu, and B. Yang, Exact landau level description of geometry and interaction in a flatband, *Phys. Rev. Lett.* **127**, 246403 (2021).
- [23] P. J. Ledwith, A. Vishwanath, and D. E. Parker, Vortexability: A unifying criterion for ideal fractional chern insulators, *Phys. Rev. B* **108**, 205144 (2023).
- [24] B. Estienne, N. Regnault, and V. Crépel, Ideal chern bands as landau levels in curved space, *Phys. Rev. Research* **5**, L032048 (2023).
- [25] Z. Liu, B. Mera, M. Fujimoto, T. Ozawa, and J. Wang, Theory of generalized landau levels and its implications for non-abelian states, *Phys. Rev. X* **15**, 031019 (2025).
- [26] R. Bistritzer and A. H. MacDonald, Moiré bands in twisted double-layer graphene, *Proc. Natl. Acad. Sci. U.S.A.* **108**, 12233 (2011).
- [27] F. Wu, T. Lovorn, E. Tutuc, and A. H. MacDonald, Hubbard model physics in transition metal dichalcogenide moiré bands, *Phys. Rev. Lett.* **121**, 026402 (2018).
- [28] F. Wu, T. Lovorn, E. Tutuc, I. Martin, and A. H. MacDonald, Topological insulators in twisted transition metal dichalcogenide homobilayers, *Phys. Rev. Lett.* **122**, 086402 (2019).
- [29] E. Y. Andrei and A. H. MacDonald, Graphene bilayers with a twist, *Nat. Mater.* **19**, 1265 (2020).
- [30] E. Y. Andrei, D. K. Efetov, P. Jarillo-Herrero, A. H. MacDonald, K. F. Mak, T. Senthil, E. Tutuc, A. Yazdani, and A. F. Young, The marvels of moiré materials, *Nat. Rev. Mater.* **6**, 201 (2021).
- [31] D. M. Kennes, M. Claassen, L. Xian, A. Georges, A. J. Millis, J. Hone, C. R. Dean, D. N. Basov, A. N. Pasupathy, and A. Rubio, Moiré heterostructures as a condensed-matter quantum simulator, *Nat. Phys.* **17**, 155 (2021).
- [32] A. Castellanos-Gomez, X. Duan, Z. Fei, H. R. Gutierrez, Y. Huang, X. Huang, *et al.*, Van der waals heterostructures, *Nat. Rev. Methods Primers* **2**, 58 (2022).
- [33] K. F. Mak and J. Shan, Semiconductor moiré materials, *Nat. Nanotechnol.* **17**, 686 (2022).
- [34] K. P. Nuckolls and A. Yazdani, A microscopic perspective on moiré materials, *Nat. Rev. Mater.* **9**, 460 (2024).
- [35] Y. Xie, A. T. Pierce, J. M. Park, D. E. Parker, E. Khalaf, P. Ledwith, Y. Cao, S. H. Lee, S. Chen, P. R. Forrester, *et al.*, Fractional chern insulators in magic-angle twisted bilayer graphene, *Nature* **600**, 439 (2021).
- [36] J. Cai, E. Anderson, C. Wang, X. Zhang, X. Liu, W. Holtzmann, Y. Zhang, F. Fan, T. Taniguchi, K. Watanabe, *et al.*, Signatures of fractional quantum anomalous hall states in twisted mote2, *Nature* **622**, 63 (2023).
- [37] Y. Zeng, Z. Xia, K. Kang, J. Zhu, P. Knüppel, C. Vaswani, K. Watanabe, T. Taniguchi, K. F. Mak, and J. Shan, Thermodynamic evidence of fractional chern insulator in moiré mote2, *Nature* **622**, 69 (2023).
- [38] H. Park, J. Cai, E. Anderson, Y. Zhang, J. Zhu, X. Liu, C. Wang, W. Holtzmann, C. Hu, Z. Liu, *et al.*, Observation of fractionally quantized anomalous hall effect, *Nature* **622**, 74 (2023).
- [39] F. Xu, Z. Sun, T. Jia, C. Liu, C. Xu, C. Li, Y. Gu, K. Watanabe, T. Taniguchi, B. Tong, *et al.*, Observation of integer and fractional quantum anomalous hall effects in twisted bilayer mote 2, *Phys. Rev. X* **13**, 031037 (2023).
- [40] E. Redekop, C. Zhang, H. Park, J. Cai, E. Anderson, O. Sheekey, T. Arp, G. Babikyan, S. Salters, K. Watanabe, T. Taniguchi, M. E. Huber, X. Xu, and A. F. Young, Direct magnetic imaging of fractional chern insulators in twisted mote2, *Nature* **635**, 584 (2024).
- [41] Z. Ji, H. Park, M. E. Barber, C. Hu, K. Watanabe, T. Taniguchi, J.-H. Chu, X. Xu, and Z.-X. Shen, Local probe of bulk and edge states in a fractional chern insulator, *Nature* **635**, 578 (2024).
- [42] F. Xu, Z. Sun, J. Li, C. Zheng, C. Xu, J. Gao, T. Jia, K. Watanabe, T. Taniguchi, B. Tong, *et al.*, Signatures of unconventional superconductivity near reentrant and fractional quantum anomalous hall insulators, *arXiv preprint arXiv:2504.06972* (2025).
- [43] Z. Lu, T. Han, Y. Yao, A. P. Reddy, J. Yang, J. Seo, K. Watanabe, T. Taniguchi, L. Fu, and L. Ju, Fractional quantum anomalous hall effect in multilayer graphene, *Nature* **626**, 759 (2024).
- [44] J. Xie, Z. Huo, X. Lu, Z. Feng, Z. Zhang, W. Wang, Q. Yang, K. Watanabe, T. Taniguchi, K. Liu, Z. Song, X. C. Xie, J. Liu, and X. Lu, Tunable fractional chern insulators in rhombohedral graphene superlattices, *Nature Materials* **24**, 1042 (2025).
- [45] Y. Choi, Y. Choi, M. Valentini, C. L. Patterson, L. F. W. Holleis, O. I. Sheekey, H. Stoyanov, X. Cheng, T. Taniguchi, K. Watanabe, and A. F. Young, Superconductivity and quantized anomalous hall effect in rhombohedral graphene, *Nature* **639**, 342 (2025).
- [46] D. Waters, A. Okounkova, R. Su, B. Zhou, J. Yao, K. Watanabe, T. Taniguchi, X. Xu, Y.-H. Zhang, J. Folk, and M. Yankowitz, Chern insulators at integer and fractional filling in moiré pentalayer graphene, *Phys. Rev. X* **15**, 011045 (2025).
- [47] S. H. Aronson, T. Han, Z. Lu, Y. Yao, J. P. Butler, K. Watanabe, T. Taniguchi, L. Ju, and R. C. Ashoori, Displacement field-controlled fractional chern insulators and charge density waves in a graphene/hbn moiré superlattice, *Phys. Rev. X* **15**, 031026 (2025).
- [48] Z. Lu, T. Han, Y. Yao, Z. Hadjri, J. Yang, J. Seo, L. Shi, S. Ye, K. Watanabe, T. Taniguchi, *et al.*, Extended quantum anomalous hall states in graphene/hbn moiré superlattices, *Nature* **637**, 1090 (2025).
- [49] W. Zhou, J. Ding, J. Hua, L. Zhang, K. Watanabe, T. Taniguchi, W. Zhu, and S. Xu, Layer-polarized ferromagnetism in rhombohedral multilayer graphene, *Nat. Commun.* **15**, 2597 (2024).
- [50] X. Han, Q. Liu, Y. Wang, R. Niu, Z. Qu, Z. Wang, Z. Li, C. Han, K. Watanabe, T. Taniguchi, Z. Song, J. Liu, J. Mao, Z. Han, B. L. Chittari, J. Jung, Z. Gan, and J. Lu, Engineering the band topology in a rhombohedral trilayer graphene moiré superlattice, *Nano Letters* **24**, 6286 (2024).
- [51] J. Ding, H. Xiang, J. Hua, W. Zhou, N. Liu, L. Zhang, N. Xin, B. Wu, K. Watanabe, T. Taniguchi, Z. c. v. Sofer, W. Zhu, and S. Xu, Electric-field switchable chirality in rhombohedral graphene chern insulators stabilized by tungsten diselenide, *Phys. Rev. X* **15**, 011052 (2025).
- [52] J. Zheng, S. Wu, K. Liu, B. Lyu, S. Liu, Y. Sha, Z. Li, K. Watanabe, T. Taniguchi, J. Jia, Z. Shi, and G. Chen, *Switchable chern insulator, isospin competitions and charge density waves in rhombohedral graphene moire superlattices* (2024), *arXiv:2412.09985 [cond-mat.str-el]*.

- [53] H. Xiang, J. Ding, J. Hua, N. Liu, W. Zhou, Q. Chen, K. Watanabe, T. Taniguchi, N. Xin, W. Zhu, and S. Xu, [Continuously tunable anomalous hall crystals in rhombohedral heptalayer graphene](#) (2025), [arXiv:2502.18031 \[cond-mat.mes-hall\]](#).
- [54] Z. Wang, Q. Liu, X. Han, Z. Li, W. Zhao, Z. Qu, C. Han, K. Watanabe, T. Taniguchi, Z. V. Han, S. Zhou, B. Tong, G. Liu, L. Lu, J. Liu, F. Wu, and J. Lu, [Electrical switching of chern insulators in moire rhombohedral heptalayer graphene](#) (2025), [arXiv:2503.00837 \[cond-mat.mes-hall\]](#).
- [55] C. Li, Z. Sun, K. Liu, L. Qiao, Y. Wei, C. Zheng, C. Zhang, K. Watanabe, T. Taniguchi, H. Yang, D. Guan, L. Liu, S. Wang, Y. Li, H. Zheng, C. Liu, B. Tong, L. Lu, J. Jia, Z. Shi, J. Liu, G. Chen, T. Li, and X. Liu, [Tunable chern insulators in moiré-distant and moiré-proximal rhombohedral pentalayer graphene](#) (2025), [arXiv:2505.01767 \[cond-mat.mes-hall\]](#).
- [56] H. Li, U. Kumar, K. Sun, and S.-Z. Lin, Spontaneous fractional chern insulators in transition metal dichalcogenide moiré superlattices, *Phys. Rev. Research* **3**, L032070 (2021).
- [57] B. Li and F. Wu, Variational mapping of chern bands to landau levels: Application to fractional chern insulators in twisted mote₂, *Phys. Rev. B* **111**, 125122 (2025).
- [58] A. P. Reddy, F. Alsallom, Y. Zhang, T. Devakul, and L. Fu, Fractional quantum anomalous hall states in twisted bilayer mote₂ and wse₂, *Phys. Rev. B* **108**, 085117 (2023).
- [59] C. Wang, X.-W. Zhang, X. Liu, Y. He, X. Xu, Y. Ran, T. Cao, and D. Xiao, Fractional chern insulator in twisted bilayer mote₂, *Phys. Rev. Lett.* **132**, 036501 (2024).
- [60] C. Xu, J. Li, Y. Xu, Z. Bi, and Y. Zhang, Maximally localized wannier functions, interaction models, and fractional quantum anomalous hall effect in twisted bilayer MoTe₂, *Proc. Natl. Acad. Sci. U.S.A.* **121**, e2316749121 (2024).
- [61] Y. Jia, J. Yu, J. Liu, J. Herzog-Arbeitman, Z. Qi, H. Pi, N. Regnault, H. Weng, B. A. Bernevig, and Q. Wu, Moiré fractional chern insulators. i. first-principles calculations and continuum models of twisted bilayer mote₂, *Phys. Rev. B* **109**, 205121 (2024).
- [62] J. Dong, J. Wang, P. J. Ledwith, A. Vishwanath, and D. E. Parker, Composite fermi liquid at zero magnetic field in twisted mote₂, *Phys. Rev. Lett.* **131**, 136502 (2023).
- [63] H. Goldman, A. P. Reddy, N. Paul, and L. Fu, Zero-field composite fermi liquid in twisted semiconductor bilayers, *Phys. Rev. Lett.* **131**, 136501 (2023).
- [64] V. Crépel and L. Fu, Anomalous hall metal and fractional chern insulator in twisted transition metal dichalcogenides, *Phys. Rev. B* **107**, L201109 (2023).
- [65] N. Morales-Durán, J. Wang, G. R. Schleder, M. Angeli, Z. Zhu, E. Kaxiras, C. Repellin, and J. Cano, Pressure-enhanced fractional chern insulators along a magic line in moiré transition metal dichalcogenides, *Phys. Rev. Research* **5**, L032022 (2023).
- [66] A. P. Reddy and L. Fu, Toward a global phase diagram of the fractional quantum anomalous hall effect, *Phys. Rev. B* **108**, 245159 (2023).
- [67] J. Yu, J. Herzog-Arbeitman, M. Wang, O. Vafek, B. A. Bernevig, and N. Regnault, Fractional chern insulators versus nonmagnetic states in twisted bilayer mote₂, *Phys. Rev. B* **109**, 045147 (2024).
- [68] C. Wang, X.-W. Zhang, X. Liu, J. Wang, T. Cao, and D. Xiao, Higher landau-level analogs and signatures of non-abelian states in twisted bilayer mote₂, *Phys. Rev. Lett.* **134**, 076503 (2025).
- [69] C. Xu, N. Mao, T. Zeng, and Y. Zhang, Multiple chern bands in twisted mote₂ and possible non-abelian states, *Phys. Rev. Lett.* **134**, 066601 (2025).
- [70] A. P. Reddy, N. Paul, A. Abouelkomsan, and L. Fu, Non-abelian fractionalization in topological minibands, *Phys. Rev. Lett.* **133**, 166503 (2024).
- [71] C.-E. Ahn, W. Lee, K. Yananose, Y. Kim, and G. Y. Cho, Non-abelian fractional quantum anomalous hall states and first landau level physics of the second moiré band of twisted bilayer mote₂, *Phys. Rev. B* **110**, L161109 (2024).
- [72] F. Chen, W.-W. Luo, W. Zhu, and D. N. Sheng, Robust non-abelian even-denominator fractional chern insulator in twisted bilayer mote₂, *Nat. Commun.* **16**, 2115 (2025).
- [73] P. Sharma, Y. Peng, and D. N. Sheng, Topological quantum phase transitions driven by a displacement field in twisted mote₂ bilayers, *Phys. Rev. B* **110**, 125142 (2024).
- [74] Y. H. Kwan, G. Wagner, J. Yu, A. K. Dagnino, Y. Jiang, X. Xu, B. A. Bernevig, T. Neupert, and N. Regnault, When could abelian fractional topological insulators exist in twisted mote₂ (and other systems), [arXiv preprint arXiv:2407.02560](#) (2024).
- [75] X. Shen, C. Wang, X. Hu, R. Guo, H. Yao, C. Wang, W. Duan, and Y. Xu, [Magnetorotons in moiré fractional chern insulators](#) (2025), [arXiv:2412.01211 \[cond-mat.str-el\]](#).
- [76] J. Chen, Q. Li, X. Wang, and W. Li, Fractional chern insulator and quantum anomalous hall crystal in twisted mote₂, [arXiv preprint arXiv:2504.07932](#) (2025).
- [77] Y. He, S. H. Simon, and S. A. Parameswaran, Fractional chern insulators and competing states in a twisted mote₂ lattice model, [arXiv preprint arXiv:2505.06354](#) (2025).
- [78] X. Li, Y. Chen, B. Li, H. Chen, F. Wu, J. Chen, and W. Ren, Deep learning sheds light on integer and fractional topological insulators, [arXiv preprint arXiv:2503.11756](#) (2025).
- [79] D. Luo, T. Zaklama, and L. Fu, Solving fractional electron states in twisted mote₂ with deep neural network, [arXiv preprint arXiv:2503.13585](#) (2025).
- [80] J. Dong, T. Wang, T. Wang, T. Soejima, M. P. Zaletel, A. Vishwanath, and D. E. Parker, Anomalous hall crystals in rhombohedral multilayer graphene. i. interaction-driven chern bands and fractional quantum hall states at zero magnetic field, *Phys. Rev. Lett.* **133**, 206503 (2024).
- [81] B. Zhou, H. Yang, and Y.-H. Zhang, Fractional quantum anomalous hall effect in rhombohedral multilayer graphene in the moiréless limit, *Phys. Rev. Lett.* **133**, 206504 (2024).
- [82] Z. Dong, A. S. Patri, and T. Senthil, Theory of quantum anomalous hall phases in pentalayer rhombohedral graphene moiré structures, *Phys. Rev. Lett.* **133**, 206502 (2024).
- [83] Z. Guo, X. Lu, B. Xie, and J. Liu, Fractional chern insulator states in multilayer graphene moiré superlattices, *Phys. Rev. B* **110**, 075109 (2024).

- [84] J. Herzog-Arbeitman, Y. Wang, J. Liu, P. M. Tam, Z. Qi, Y. Jia, D. K. Efetov, O. Vafek, N. Regnault, H. Weng, Q. Wu, B. A. Bernevig, and J. Yu, Moiré fractional chern insulators. ii. first-principles calculations and continuum models of rhombohedral graphene superlattices, *Phys. Rev. B* **109**, 205122 (2024).
- [85] Y. H. Kwan, J. Yu, J. Herzog-Arbeitman, D. K. Efetov, N. Regnault, and B. A. Bernevig, Moiré fractional chern insulators. iii. hartree-fock phase diagram, magic angle regime for chern insulator states, role of moiré potential, and goldstone gaps in rhombohedral graphene superlattices, *Phys. Rev. B* **112**, 075109 (2025).
- [86] Z. Dong, A. S. Patri, and T. Senthil, Stability of anomalous hall crystals in multilayer rhombohedral graphene, *Phys. Rev. B* **110**, 205130 (2024).
- [87] T. Soejima, J. Dong, T. Wang, T. Wang, M. P. Zaletel, A. Vishwanath, and D. E. Parker, Anomalous hall crystals in rhombohedral multilayer graphene. ii. general mechanism and a minimal model, *Phys. Rev. B* **110**, 205124 (2024).
- [88] T. Tan and T. Devakul, Parent berry curvature and the ideal anomalous hall crystal, *Phys. Rev. X* **14**, 041040 (2024).
- [89] Y. Zeng, D. Guerci, V. Crépel, A. J. Millis, and J. Cano, Sublattice structure and topology in spontaneously crystallized electronic states, *Phys. Rev. Lett.* **132**, 236601 (2024).
- [90] M. Xie and S. Das Sarma, Integer and fractional quantum anomalous hall effects in pentalayer graphene, *Phys. Rev. B* **109**, L241115 (2024).
- [91] V. Crépel and J. Cano, Efficient prediction of superlattice and anomalous miniband topology from quantum geometry, *Phys. Rev. X* **15**, 011004 (2025).
- [92] K. Kudo, R. Nakai, and K. Nomura, Quantum anomalous, spin, and valley hall effects in pentalayer rhombohedral graphene moiré superlattices, *Phys. Rev. B* **110**, 245135 (2024).
- [93] S. Das Sarma and M. Xie, Thermal crossover from a chern insulator to a fractional chern insulator in pentalayer graphene, *Phys. Rev. B* **110**, 155148 (2024).
- [94] K. Huang, X. Li, S. Das Sarma, and F. Zhang, Self-consistent theory of fractional quantum anomalous hall states in rhombohedral graphene, *Phys. Rev. B* **110**, 115146 (2024).
- [95] J. Yu, J. Herzog-Arbeitman, Y. H. Kwan, N. Regnault, and B. A. Bernevig, Moiré fractional chern insulators. iv. fluctuation-driven collapse in multiband exact diagonalization calculations on rhombohedral graphene, *Phys. Rev. B* **112**, 075110 (2025).
- [96] G. Shavit, Entropy-enhanced fractional quantum anomalous hall effect, *Phys. Rev. B* **110**, L201406 (2024).
- [97] K. Huang, S. Das Sarma, and X. Li, Fractional quantum anomalous hall effect in rhombohedral multilayer graphene with a strong displacement field, *Phys. Rev. B* **111**, 075130 (2025).
- [98] K. Huang, S. D. Sarma, and X. Li, Impurity-induced thermal crossover in fractional chern insulators (2024), [arXiv:2409.04349 \[cond-mat.str-el\]](https://arxiv.org/abs/2409.04349).
- [99] Z. Guo and J. Liu, Beyond-mean-field studies of wigner crystal transitions in various interacting two-dimensional systems (2024), [arXiv:2409.14658 \[cond-mat.str-el\]](https://arxiv.org/abs/2409.14658).
- [100] Z. Wei, A.-K. Wu, M. Gonçalves, and S.-Z. Lin, Edge-driven transition between extended quantum anomalous hall crystal and fractional chern insulator in rhombohedral graphene multilayers, *Phys. Rev. B* **111**, 035116 (2025).
- [101] T. Tan, J. May-Mann, and T. Devakul, Variational wave-function analysis of the fractional anomalous hall crystal, *Phys. Rev. Lett.* **135**, 036604 (2025).
- [102] B. Zhou and Y.-H. Zhang, New classes of quantum anomalous hall crystals in multilayer graphene, *Phys. Rev. Lett.* **135**, 036501 (2025).
- [103] Y. Zeng and A. J. Millis, Berry phase dynamics of sliding electron crystals, *Phys. Rev. X* **15**, 031059 (2025).
- [104] H. Li, B. A. Bernevig, and N. Regnault, Multiband exact diagonalization and an iteration approach to search for fractional chern insulators in rhombohedral multilayer graphene, *Phys. Rev. B* **112**, 075130 (2025).
- [105] M. Uzan, W. Zhi, M. Bocarsly, J. Dong, S. Dutta, N. Auerbach, N. S. Kander, M. Labendik, Y. Myasodov, M. E. Huber, K. Watanabe, T. Taniguchi, D. E. Parker, and E. Zeldov, hbn alignment orientation controls moiré strength in rhombohedral graphene (2025), [arXiv:2507.20647 \[cond-mat.mes-hall\]](https://arxiv.org/abs/2507.20647).
- [106] Z. Huo, W. Wang, J. Xie, Y. H. Kwan, J. Herzog-Arbeitman, Z. Zhang, Q. Yang, M. Wu, K. Watanabe, T. Taniguchi, K. Liu, N. Regnault, B. A. Bernevig, and X. Lu, Does moire matter? critical moire dependence with quantum fluctuations in graphene based integer and fractional chern insulators (2025), [arXiv:2510.15309 \[cond-mat.mes-hall\]](https://arxiv.org/abs/2510.15309).
- [107] X.-Y. Song, C.-M. Jian, L. Fu, and C. Xu, Intertwined fractional quantum anomalous hall states and charge density waves, *Phys. Rev. B* **109**, 115116 (2024).
- [108] X.-Y. Song and T. Senthil, Density wave halo around anyons in fractional quantum anomalous hall states, *Phys. Rev. B* **110**, 085120 (2024).
- [109] D. N. Sheng, A. P. Reddy, A. Abouelkomsan, E. J. Bergholtz, and L. Fu, Quantum anomalous hall crystal at fractional filling of moiré superlattices, *Phys. Rev. Lett.* **133**, 066601 (2024).
- [110] H. Pan, M. Xie, F. Wu, and S. Das Sarma, Topological phases in ab-stacked $\text{mote}_2/\text{wse}_2$: F_2 topological insulators, chern insulators, and topological charge density waves, *Phys. Rev. Lett.* **129**, 056804 (2022).
- [111] Z. Dong, A. S. Patri, and T. Senthil, Theory of quantum anomalous hall phases in pentalayer rhombohedral graphene moiré structures, *Phys. Rev. Lett.* **133**, 206502 (2024).
- [112] B. Zhou, H. Yang, and Y.-H. Zhang, Fractional quantum anomalous hall effect in rhombohedral multilayer graphene in the moiréless limit, *Phys. Rev. Lett.* **133**, 206504 (2024).
- [113] J. Dong, T. Wang, T. Wang, T. Soejima, M. P. Zaletel, A. Vishwanath, and D. E. Parker, Anomalous hall crystals in rhombohedral multilayer graphene. i. interaction-driven chern bands and fractional quantum hall states at zero magnetic field, *Phys. Rev. Lett.* **133**, 206503 (2024).
- [114] Y. H. Kwan, J. Yu, J. Herzog-Arbeitman, D. K. Efetov, N. Regnault, and B. A. Bernevig, Moiré fractional chern insulators. iii. hartree-fock phase diagram, magic angle regime for chern insulator states, role of moiré potential, and goldstone gaps in rhombohedral graphene superlattices, *Phys. Rev. B* **112**, 075109 (2025).
- [115] T. Tan and T. Devakul, Parent berry curvature and the

- ideal anomalous hall crystal, *Phys. Rev. X* **14**, 041040 (2024).
- [116] T. Soejima, J. Dong, T. Wang, T. Wang, M. P. Zaletel, A. Vishwanath, and D. E. Parker, Anomalous hall crystals in rhombohedral multilayer graphene. ii. general mechanism and a minimal model, *Phys. Rev. B* **110**, 205124 (2024).
- [117] Z. Dong, A. S. Patri, and T. Senthil, Stability of anomalous hall crystals in multilayer rhombohedral graphene, *Phys. Rev. B* **110**, 205130 (2024).
- [118] S. R. White, Density matrix formulation for quantum renormalization groups, *Phys. Rev. Lett.* **69**, 2863 (1992).
- [119] S. R. White, Density-matrix algorithms for quantum renormalization groups, *Phys. Rev. B* **48**, 10345 (1993).
- [120] U. Schollwöck, The density-matrix renormalization group in the age of matrix product states, *Ann. Phys.* **326**, 96 (2011).
- [121] T. Devakul, V. Crépel, Y. Zhang, and L. Fu, Magic in twisted transition metal dichalcogenide bilayers, *Nat. Commun.* **12**, 6730 (2021).
- [122] W.-X. Qiu, B. Li, X.-J. Luo, and F. Wu, Interaction-driven topological phase diagram of twisted bilayer MoTe_2 , *Phys. Rev. X* **13**, 041026 (2023).
- [123] V. Crépel and A. Millis, Bridging the small and large in twisted transition metal dichalcogenide homobilayers: A tight binding model capturing orbital interference and topology across a wide range of twist angles, *Phys. Rev. Research* **6**, 033127 (2024).
- [124] See supplemental material.
- [125] E. Anderson, F.-R. Fan, J. Cai, W. Holtzmann, T. Taniguchi, K. Watanabe, D. Xiao, W. Yao, and X. Xu, Programming correlated magnetic states with gate-controlled moiré geometry, *Science* **381**, 325 (2023).
- [126] F. D. M. Haldane, Model for a quantum hall effect without landau levels: Condensed-matter realization of the "parity anomaly", *Phys. Rev. Lett.* **61**, 2015 (1988).
- [127] R. B. Laughlin, Quantized hall conductivity in two dimensions, *Phys. Rev. B* **23**, 5632 (1981).
- [128] D. J. Thouless, M. Kohmoto, M. P. Nightingale, and M. den Nijs, Quantized hall conductance in a two-dimensional periodic potential, *Phys. Rev. Lett.* **49**, 405 (1982).
- [129] Q. Niu, D. J. Thouless, and Y.-S. Wu, Quantized hall conductance as a topological invariant, *Phys. Rev. B* **31**, 3372 (1985).
- [130] M. P. Zaletel, R. S. K. Mong, and F. Pollmann, Topological characterization of fractional quantum hall ground states from microscopic hamiltonians, *Phys. Rev. Lett.* **110**, 236801 (2013).
- [131] R. B. Laughlin, Superconducting ground state of non-interacting particles obeying fractional statistics, *Phys. Rev. Lett.* **60**, 2677 (1988).
- [132] D.-H. Lee and M. P. A. Fisher, Anyon superconductivity and the fractional quantum hall effect, *Phys. Rev. Lett.* **63**, 903 (1989).
- [133] S. Divic, V. Crépel, T. Soejima, X.-Y. Song, A. J. Millis, M. P. Zaletel, and A. Vishwanath, Anyon superconductivity from topological criticality in a hofstadter-hubbard model, *Proceedings of the National Academy of Sciences* **122**, e2426680122 (2025).
- [134] T. Wang and M. P. Zaletel, Chiral superconductivity near a fractional chern insulator (2025), [arXiv:2507.07921 \[cond-mat.str-el\]](https://arxiv.org/abs/2507.07921).
- [135] C. Kuhlenkamp, S. Divic, M. P. Zaletel, T. Soejima, and A. Vishwanath, Robust superconductivity upon doping chiral spin liquid and chern insulators in a hubbard-hofstadter model (2025), [arXiv:2509.02675 \[cond-mat.str-el\]](https://arxiv.org/abs/2509.02675).
- [136] F. Pichler, C. Kuhlenkamp, M. Knap, and A. Vishwanath, Microscopic mechanism of anyon superconductivity emerging from fractional chern insulators, *Newton*, 100340 (2025).
- [137] P. A. Nosov, Z. Han, and E. Khalaf, Anyon superconductivity and plateau transitions in doped fractional quantum anomalous hall insulators (2025), [arXiv:2506.02108 \[cond-mat.str-el\]](https://arxiv.org/abs/2506.02108).
- [138] Z. D. Shi and T. Senthil, Doping a fractional quantum anomalous hall insulator, *Phys. Rev. X* **15**, 031023 (2025).
- [139] Z. D. Shi and T. Senthil, Anyon delocalization transitions out of a disordered fqah insulator (2025), [arXiv:2506.02128 \[cond-mat.str-el\]](https://arxiv.org/abs/2506.02128).
- [140] Z. D. Shi and T. Senthil, Non-abelian topological superconductivity from melting abelian fractional chern insulators (2025), [arXiv:2512.17996 \[cond-mat.str-el\]](https://arxiv.org/abs/2512.17996).
- [141] D. Guerci, A. Abouelkomsan, and L. Fu, From fractionalization to chiral topological superconductivity in a flat chern band (2025), [arXiv:2506.10938 \[cond-mat.supr-con\]](https://arxiv.org/abs/2506.10938).

Supplemental material for ‘Fractional quantum anomalous Hall and anyon density-wave halo in a minimal interacting lattice model of twisted bilayer MoTe₂’

Chuyi Tuo,¹ Ming-Rui Li,¹ and Hong Yao^{1,*}

¹*Institute for Advanced Study, Tsinghua University, Beijing 100084, China*

(Dated: December 30, 2025)

I. CONSTRUCTION OF THE WANNIER FUNCTIONS

In this section, we provide details of the procedure for constructing the Wannier functions. Our starting point is the continuum model [1] for *t*MoTe₂, where the Hamiltonian for *K* valley is given by:

$$H_K(\mathbf{r}) = \begin{pmatrix} -\frac{\hbar^2(\mathbf{k}-\boldsymbol{\kappa}_+)^2}{2m^*} + \Delta_+(\mathbf{r}) & \Delta_T(\mathbf{r}) \\ \Delta_T^\dagger(\mathbf{r}) & -\frac{\hbar^2(\mathbf{k}-\boldsymbol{\kappa}_-)^2}{2m^*} + \Delta_-(\mathbf{r}) \end{pmatrix}. \quad (\text{S1})$$

Here $m^* = 0.6m_e$ is the effective mass of monolayer MoTe₂, $\boldsymbol{\kappa}_\pm$ denote the wave vectors of the mini Brillouin zone corners. The moiré potential $\Delta_\pm(\mathbf{r})$ and interlayer tunneling $\Delta_T(\mathbf{r})$ are given by:

$$\Delta_\pm(\mathbf{r}) = 2v \sum_{j=1,3,5} \cos(\mathbf{g}_j \cdot \mathbf{r} \pm \psi) \quad (\text{S2})$$

$$\Delta_T(\mathbf{r}) = w (1 + e^{-i\mathbf{g}_2 \cdot \mathbf{r}} + e^{-i\mathbf{g}_3 \cdot \mathbf{r}}) \quad (\text{S3})$$

and the moiré wave vectors \mathbf{g}_j are obtained by rotation of $\mathbf{g}_1 = (\frac{4\pi}{\sqrt{3}a_M}, 0)$ by $(j-1)\pi/3$. The continuum model parameters are obtained by large scale ab initio simulations $(v, \psi, w) = (20.8\text{meV}, 107.7^\circ, -23.8\text{meV})$ [2]. Here we focus on the experimentally relevant twist angle $\theta = 3.7^\circ$, and the moiré lattice constant is given by $a_M \approx a_0/\theta$ with $a_0 = 3.52\text{\AA}$. Motivated by the robust experimental evidence for spin-valley polarization ferromagnetism [3] in the FQAH regime of interest, we restrict our attention to consider spinless fermion at *K* valley in this paper. And, as stated in the main text, we consider the top two moiré valence bands to eliminate the topological Wannier obstruction.

We construct exponentially localized Wannier functions in a particularly convenient manner [4–7] by exploiting the layer polarization properties of *t*MoTe₂. In our case of 3.7° *t*MoTe₂, the Wannier centers are located at XM and MX regions, and the associated Wannier functions are polarized on opposite layers as a consequence of the large metal-chalcogenide chemical potential difference. The Wannierization procedure utilizing the layer polarization properties is described as follows: (i) diagonalize the continuum model in momentum space to obtain the Bloch eigenstates $|\phi_{n\mathbf{k}}\rangle$, where $n = 1, 2$ is the band index; (ii) construct the layer polarization operator $P_{nn'}(\mathbf{k}) = \langle \phi_{n\mathbf{k}} | \tau^z | \phi_{n'\mathbf{k}} \rangle$, where τ^z denotes the *z* component of the layer pseudospin. (iii) diagonalize the layer polarization operator $P_{nn'}(\mathbf{k})$ at each momentum \mathbf{k} via a unitary transformation $U_{nn'}(\mathbf{k})$, and the resulting two eigenstates $|\tilde{\phi}_{n\mathbf{k}}\rangle = \sum_{n'} U_{nn'}(\mathbf{k}) |\phi_{n'\mathbf{k}}\rangle$ are predominantly polarized on opposite layers. (iv) fix the gauge of each $|\tilde{\phi}_{n\mathbf{k}}\rangle$ by imposing it to be real and positive at the corresponding Wannier centers (i.e. XM or MX regions $(\pm a_M/2\sqrt{3}, 0)$). (v) the Wannier functions at lattice vector \mathbf{R} can then be constructed by $|W_{n\mathbf{R}}\rangle = \frac{1}{\sqrt{N}} \sum_{\mathbf{k}} e^{-i\mathbf{k} \cdot \mathbf{R}} |\tilde{\phi}_{n\mathbf{k}}\rangle$, where N is the total number of unit cells. The resulting Wannier functions are illustrated in Fig. 1(a) in the main text, which are well exponentially localized and display the correct layer polarization and Wannier center locations.

II. ADIABATIC CHARGE PUMPING

In this section, we provide additional details on the adiabatic charge pumping method [8–11] adopted in the main text, which serves as an indispensable numerical tool for accessing the topological properties of the many-body ground state in our DMRG simulations on cylinder geometry. In simple terms, adiabatically threading flux Φ through the cylinder induces an electric field along the circumferential direction, which the Hall response converts into a transverse current along the cylinder axis, resulting in a net charge transfer between the two open edges in proportional to the Hall conductance σ_{xy} . The quantization of the Hall conductance σ_{xy} in a gapped phase can also be understood straightforwardly from gauge invariance under insertion of integer number of 2π flux quanta.

Practically, flux insertion is implemented by imposing twisted boundary conditions around the circumference of the cylinder, i.e., $c_{x,y+L_y}^\dagger = e^{i\Phi} c_{x,y}^\dagger$ when writing in terms of the brick-wall coordinate of the honeycomb lattice. Therefore, the hopping terms acquire a phase $+\Phi$ when crossing the circumferential boundary in the positive direction, and a phase $-\Phi$ when crossing in the opposite direction, while other terms in the Hamiltonian remain invariant. In our DMRG simulations, adiabatic charge pumping is implemented as follows: (i) the 2π flux insertion is discretized into M steps, where $\Phi_m = 2\pi m/M$ with $m = 0, \dots, M$; (ii) for each flux value Φ_m , we compute the many-body ground state of the Hamiltonian $H(\Phi_m)$, using the converged ground state at Φ_{m-1} as the initial state to ensure adiabatic continuity; (iii) at each Φ_m , we measure the real-space density profile to extract the pumped charge. In our simulations, since the ground state is intertwined with charge orders, a sufficiently slow flux insertion (i.e., a relatively large M) is required to ensure numerical reliability.

In the main text, we have provided robust numerical evidences for the quantization of Hall conductance σ_{xy} in various phases. Here, we present additional real space information associated with these adiabatic charge pumping processes. Figures S1 and S2 illustrate the adiabatic charge pumping for the FQAH and QAHC phases with several representative values of the flux Φ , showing that the density changes occur predominantly at the edges while the bulk remains stable. In contrast, Fig. S3 illustrates that the topologically trivial CDW phase exhibits almost no response to the inserted flux. These results suggest that adiabatic charge pumping serves as a powerful and direct numerical probe of the topological properties for the many-body ground state.

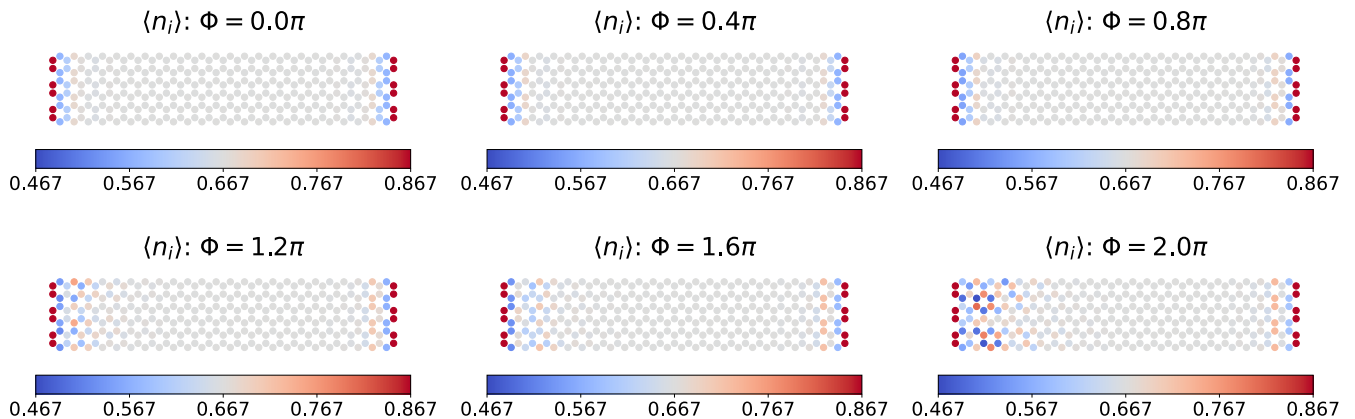


FIG. S1. Density distributions for representative flux values in the FQAH phase with $V_1 = 8$ meV.

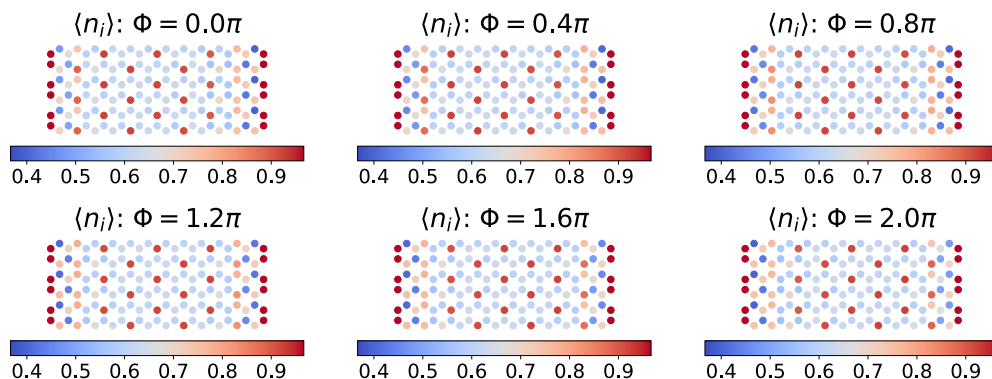


FIG. S2. Density distributions for representative flux values in the QAHC phase with $V_1 = 10$ meV, $V_2 = 3$ meV, $D = 1$ meV.

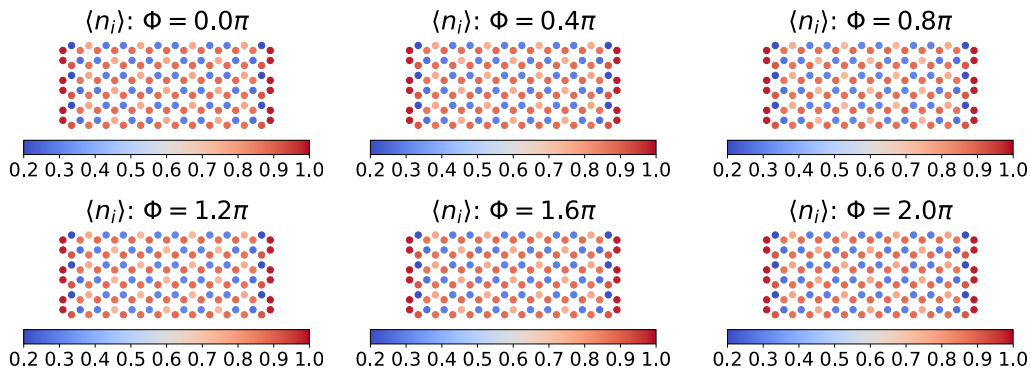


FIG. S3. Density distributions for representative flux values in the CDW phase with $V_1 = 10$ meV, $V_2 = 3$ meV, $D = 5$ meV.

III. ANYON DENSITY-WAVE HALO CLOSE TO THE FQAH-QAHC TRANSITION

In the main text, we have demonstrated that anyon density-wave halo [12] can occur in systems with only NN interaction V_1 . Here, we provide additional numerical evidence that such phenomena also persist in the presence of finite NNN interaction V_2 and displacement field D close to the FQAH-QAHC transition. Fig. S4(a) illustrates the real space density distribution $\langle n_i \rangle$ for a representative system close to the FQAH-QAHC transition at $V_1 = 10$ meV, $V_2 = 1.5$ meV, $D = 1$ meV, where an additional electron relative to the $\nu = -2/3$ filling is included to compensate for the open boundary effects. While most of the bulk shows sublattice staggered density modulation induced by the displacement field, the central region of the bulk develops $\sqrt{3} \times \sqrt{3}$ CDW pattern similar to the QAHC phase (see Fig. 4(c) in the main text), which is consistent with an anyon density-wave halo. To obtain decisive evidence that this density modulation is associated with an anyon, we compute the cumulative sum of the density deviation $\langle n_i \rangle - 2/3$ measured from the left boundary, as shown in Fig. S4(b). From this cumulative sum, we find that the extra electron fractionalizes, resulting in a net charge of $-1/3$ associated with the anyon density-wave halo in the bulk, as well as an excess charge of $2/3$ at each open edge. These results provide strong evidence that anyon density-wave halos persist over a broad parameter regime in $t\text{MoTe}_2$ and encode the characteristics of nearby charge ordered phases, highlighting the close interplay between the FQAH state and proximate ordered phases.

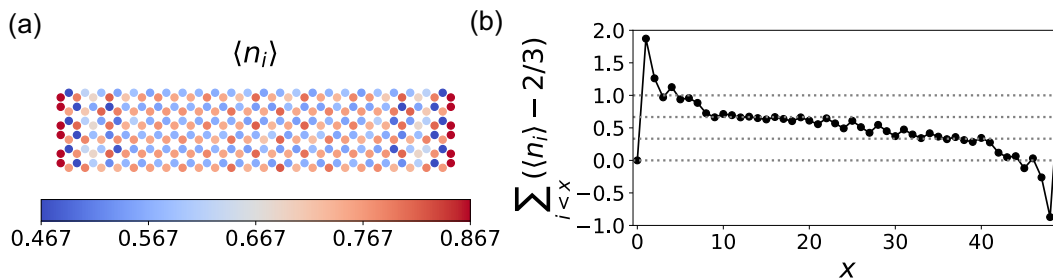


FIG. S4. (a) Density distribution for system with $V_1 = 10$ meV, $V_2 = 1.5$ meV, $D = 1$ meV, showing a clear anyon density-wave halo with $\sqrt{3} \times \sqrt{3}$ CDW pattern. (b) Cumulative sum of the density deviation $\langle n_i \rangle - 2/3$ from the left boundary, and the gray dashed lines mark values of 0, $1/3$, $2/3$, 1.

* yaohong@tsinghua.edu.cn

- [1] F. Wu, T. Lovorn, E. Tutuc, I. Martin, and A. H. MacDonald, Topological insulators in twisted transition metal dichalcogenide homobilayers, *Phys. Rev. Lett.* **122**, 086402 (2019).
- [2] C. Wang, X.-W. Zhang, X. Liu, Y. He, X. Xu, Y. Ran, T. Cao, and D. Xiao, Fractional chern insulator in twisted bilayer mote_2 , *Phys. Rev. Lett.* **132**, 036501 (2024).

- [3] E. Anderson, F.-R. Fan, J. Cai, W. Holtzmann, T. Taniguchi, K. Watanabe, D. Xiao, W. Yao, and X. Xu, Programming correlated magnetic states with gate-controlled moiré geometry, *Science* **381**, 325 (2023).
- [4] T. Devakul, V. Crépel, Y. Zhang, and L. Fu, Magic in twisted transition metal dichalcogenide bilayers, *Nat. Commun.* **12**, 6730 (2021).
- [5] W.-X. Qiu, B. Li, X.-J. Luo, and F. Wu, Interaction-driven topological phase diagram of twisted bilayer MoTe₂, *Phys. Rev. X* **13**, 041026 (2023).
- [6] C. Xu, J. Li, Y. Xu, Z. Bi, and Y. Zhang, Maximally localized wannier functions, interaction models, and fractional quantum anomalous hall effect in twisted bilayer MoTe₂, *Proc. Natl. Acad. Sci. U.S.A.* **121**, e2316749121 (2024).
- [7] V. Crépel and A. Millis, Bridging the small and large in twisted transition metal dichalcogenide homobilayers: A tight binding model capturing orbital interference and topology across a wide range of twist angles, *Phys. Rev. Research* **6**, 033127 (2024).
- [8] R. B. Laughlin, Quantized hall conductivity in two dimensions, *Phys. Rev. B* **23**, 5632 (1981).
- [9] D. J. Thouless, M. Kohmoto, M. P. Nightingale, and M. den Nijs, Quantized hall conductance in a two-dimensional periodic potential, *Phys. Rev. Lett.* **49**, 405 (1982).
- [10] Q. Niu, D. J. Thouless, and Y.-S. Wu, Quantized hall conductance as a topological invariant, *Phys. Rev. B* **31**, 3372 (1985).
- [11] M. P. Zaletel, R. S. K. Mong, and F. Pollmann, Topological characterization of fractional quantum hall ground states from microscopic hamiltonians, *Phys. Rev. Lett.* **110**, 236801 (2013).
- [12] X.-Y. Song and T. Senthil, Density wave halo around anyons in fractional quantum anomalous hall states, *Phys. Rev. B* **110**, 085120 (2024).